Photoacoustics 2 (2014) 81–86

Contents lists available at ScienceDirect

Photoacoustics

journal homepage: www.elsevier.com/locate/pacs

Short Communication

In vivo corneal neovascularization imaging by optical-resolution photoacoustic microscopy

Wenzhong Liu [a], Kathryn M. Schultz [b], Kevin Zhang [a], Amy Sasman [b], Fengli Gao [a,c], Tsutomu Kume [b,*], Hao F. Zhang [a,d,**]

[a] Department of Biomedical Engineering, Northwestern University, Evanston, IL 60208, USA
[b] Feinberg Cardiovascular Research Institute, Feinberg School of Medicine, Northwestern University, Chicago, IL 60611, USA
[c] State Key Laboratory on Integrated Optoelectronics, College of Electronic Science and Engineering, Jilin University, Changchun 130012, China
[d] Department of Ophthalmology, Northwestern University, Chicago, IL 60611, USA

ARTICLE INFO

Article history:
Received 8 November 2013
Received in revised form 2 April 2014
Accepted 8 April 2014
Available online 21 April 2014

Keywords:
Photoacoustic microscopy
Cornea
Neovascularization

ABSTRACT

Corneal neovascularization leads to blurred vision, thus *in vivo* visualization is essential for pathological studies in animal models. Photoacoustic (PA) imaging can delineate microvasculature and hemodynamics noninvasively, which is suitable for investigating corneal neovascularization. In this study, we demonstrate *in vivo* imaging of corneal neovascularization in the mouse eye by optical-resolution photoacoustic microscopy (OR-PAM), where corneal neovascularization is induced by deliberate alkali burn injuries in C57BL6/J inbred mice corneas on the left eye. We used OR-PAM to image five mice with corneal alkali burn injuries; the uninjured eyes (right eye) in these mice are then used as the controls. Corneal images acquired by OR-PAM with and without alkali burn injury are compared, clear signs of corneal neovascularization are present in the OR-PAM images of injured eyes; the OR-PAM results are also confirmed by postmortem fluorescence-labeled confocal microscopy.

1. Introduction

Normal corneal tissue is avascular in order to allow light to pass through without being affected; the presence of blood vessels in the cornea, usually as a result of corneal neovascularization, can partially obstruct incoming light, leading to blurred vision. This pathophysiology has been observed in humans most commonly as a form of inflammatory response to an external insult [1] or as a less common but more serious autoimmune response such as Cogan's syndrome [2]. Without treatment, the progression of corneal neovascularization can completely block light from entering the eye [3].

Visualization of the vascular cornea is important for a pathological study of corneal neovascularization, as well as monitoring its disease progression in animal models. Current methods of visualizing corneal neovascularization *in vivo* include slit lamp imaging [4,5] and confocal microscopy imaging [6]. Slit lamp imaging can be performed with computerized color image analysis [4] or with fluorescent angiography [5]. Color image analysis is subjective and therefore limited. Fluorescent angiography, although repeatable, requires that subjects be tolerant to injectable chemical dyes. Confocal microscopy imaging boasts high resolution [7], but as a light scattering or fluorescence contrast based method, is not yet able to quantify the oxygen saturation level within vessels, which is important for identifying the progression of microvascular related diseases and viability of the tissue [8].

One potential effective imaging modality for corneal neovascularization visualization is photoacoustic microscopy (PAM), which takes advantage of the strong optical absorption of hemoglobin to image microvascular networks with a high image contrast and high spatial resolution [9]. In PAM, short laser pulses are directed into biological tissues [8,10,11,12,13]; when chromospheres, such as hemoglobin and melanin, absorb optical energy, thermoelastic vibration will be triggered in corresponding tissues and as a result, generation of broadband ultrasonic waves occur [10,12,14]. Such ultrasonic waves, carrying information of the optical absorption properties, geometry, and location of local tissues, can be detected for microscopic imaging; when multi-wavelength illumination is used, PAM can also assess blood oxygen

* Corresponding author at: Feinberg Cardiovascular Research Institute, Feinberg School of Medicine, Northwestern University, Chicago, IL 60611, USA. Tel.: +13126954965.
** Corresponding author at: Department of Biomedical Engineering, Northwestern University, Evanston, IL 60208, USA. Tel.: +18474912946.
E-mail addresses: t-kume@northwestern.edu (T. Kume), hfzhang@northwestern.edu (H.F. Zhang).

http://dx.doi.org/10.1016/j.pacs.2014.04.003

saturation, and thus can potentially detect the onset of diseases associated with microvascular pathologies [15,16]. Recently, applications of PAM have been demonstrated in cardiovascular pathophysiologies [17,18,19], diabetes [20] brain trauma [21], tumor angiogenesis [8,13,22] and iris vascular networks [23].

In this paper we report on the application of optical-resolution PAM (OR-PAM) to image corneal neovascularization. We first deliberately induced corneal neovascularization in C57BL6/J inbred mice by chemically burning the right cornea with an alkaline solution [24]. Two weeks later, we subjected them to our OR-PAM system for corneal imaging. We imaged the left eye of five mice to gauge the progression of angiogenesis and used the uninjured right eyes as controls. Clear signs of corneal neovascularization were observed in the injured eyes using OR-PAM; but not in the control eyes. The OR-PAM results were also confirmed by postmortem histological examination using fluorescence confocal microscopy.

2. Materials and methods

2.1. OR-PAM system

The schematic diagram of OR-PAM is shown in Fig. 1a. An Nd:YAG laser (SPOT-10-200-532, Elforlight Ltd.; output wavelength: 532 nm; pulse duration: 1 ns) served as the illumination source. The laser output was delivered by a single-mode optical fiber, further filtered by a 75 μm diameter pinhole (P75S, Thorlabs) and collimated to 9 mm in diameter through a telescope system; then the laser was focused by a microscope objective (PlanN4×, NA = 0.1, Olympus) onto the sample through a beam splitter cube (reflectance/transmittance ratio: 70/30). Laser-induced ultrasonic signals were firstly collimated coaxially with the illumination laser light through a plano-concave lens (Diameter: 6.0 mm, Focal length: 9 mm, Edmund Optics) attached to the bottom of the beam-splitter cube; and then detected by an unfocused ultrasonic transducer (V312, Olympus NDT; center frequency: 10 MHz; bandwidth: 80%; active element diameter: 6 mm). The detected PA signals were amplified by a wideband amplifier (ZFL 500LN, Mini-Circuits); then digitized and recorded by an acquisition board (CS12400, Gage Applied) at a sampling rate of 400MS/s. During imaging, the mouse was placed on an x–y motorized stage (23H118S059, Danaher Motion). A custom-made water tank with a window at the bottom (sealed by a thin plastic membrane) was used for ultrasonic coupling between the mouse eye and detection.

To test the lateral resolution of our OR-PAM system, we imaged a USAF resolution target (USAF-1951, Applied Image). The OR-PAM system can resolve the fourth element of group 7 (Fig. 1b), which corresponds to a lateral resolution of 2.76 μm and a Rayleigh length of 11.5 μm at 532 nm. To determine the axial resolution, a typical A-line (Fig. 1c) was used as the approximation of a 1D acoustic axial point-spread-function (PSF). We shifted the 1D PSF with a distance and added it back to the original PSF. We then applied Rayleigh criterion to the sum, where the smallest shifted distance capable of resolving two peaks in the sum (by a 10%

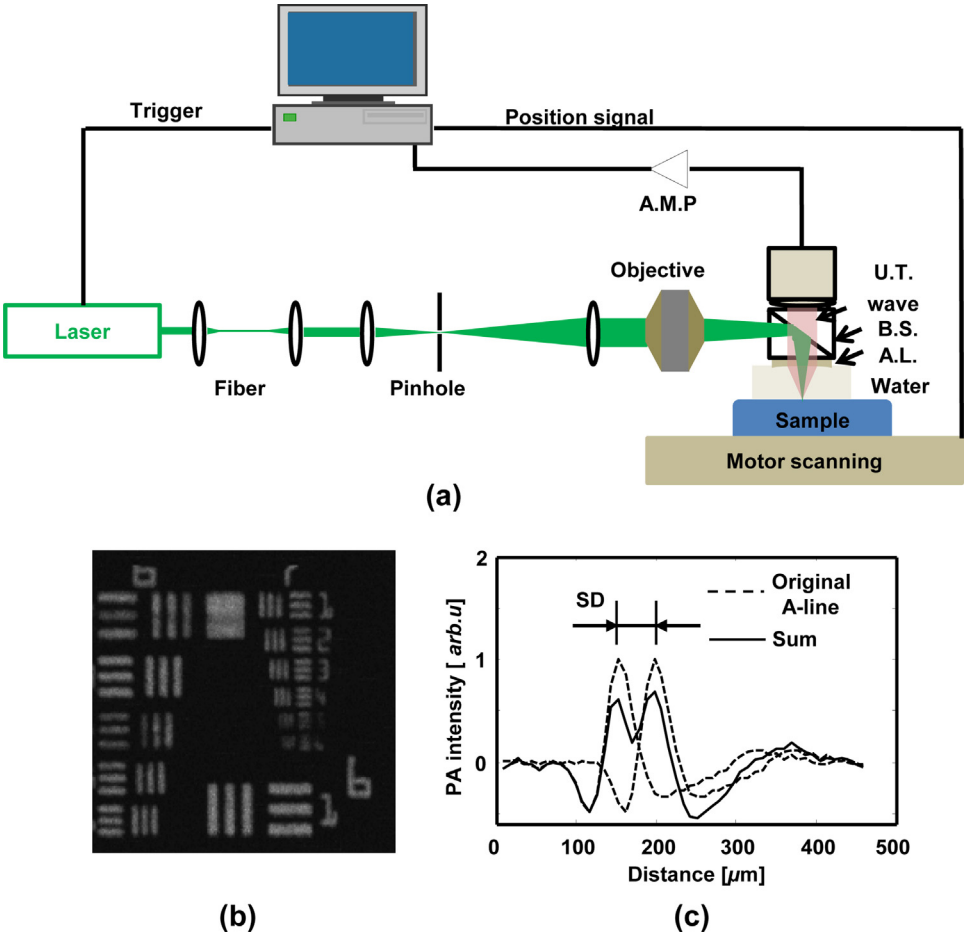

Fig. 1. Experimental OR-PAM system. (a) Schematic of the OR-PAM system; AMP: amplifier; UT: ultrasonic transducer; BS: beam splitter; AL: acoustic lens; (b) maximum amplitude projection OR-PAM image of a USAF-1951 resolution target; (c) estimation of axial resolution from a typical A-line acquired from USAF-1951 target. SD: shift difference.

amplitude difference) was considered as the axial resolution [25]. As shown in Fig. 1c, the axial resolution for our OR-PAM system is around 50 μm.

In our experiments, the laser pulse energy was 80 nJ. The radiant exposure within the focal spot was 13.4 mJ/cm^2, which was within the maximum permissible exposure limit determined by the American National Standards Institute (ANSI) [26]. The laser induced temperature rise in biological tissue was estimated to be on the order of milliKelvins (mK) [27], which is considered safe.

2.2. Anatomy of corneal structure and corneal neovascularization

As shown in Fig. 2, a typical health mouse cornea consists of an avascular transparent structure in an arc shape located at the foremost anterior segment of the eyeball. Parts of the anterior eye adjacent to the cornea include the conjunctiva, iris, limbus and sclera. The typical curvature of a mouse cornea is 1.4 mm [28], with 60 μm in thickness [28]. When the cornea becomes injured, there exists abnormal growth of blood vessels from the limbus into the adjacent corneal stroma as marked by the red arrows in Fig. 2. This will most likely result in vision debilitation and obstruction.

2.2.1. Animal model preparation and corneal imaging

In an effort to elucidate the injury-mediated vascular outgrowth from the limbus into the cornea, we injured the wild-type C57BL6/J mice corneas as previously described [29]. Briefly, at 6-weeks old, mice were anesthetized by intraperitoneal (IP) injection of a solution of ketamine hydrochloride (80 mg/kg body weight; Fort Dodge Animal Health) and xylazine (6 mg/kg body weight; Lloyd Laboratories). The cornea was further desensitized with a 0.5% proparacaine hydrochloride ophthalmic solution (Bausch & Laumb) for 1 minute. Then 2 mm disks soaked with 1-N sodium hydroxide were placed on the cornea for 1 min. The corneas were then flushed with saline and treated with erythromycin ophthalmic ointment (Fougera) to prevent bacterial infections. At the 14th day after injury, the corneas were imaged by OR-PAM, and then harvested for histological analysis.

For corneal imaging, we first anesthetized the mouse by an intraperitoneal (IP) injection of a cocktail of Ketamine (87 mg/kg body weight) and Xylazine (13 mg/kg body weight). We then applied a 0.5% Tetracaine Hydrochloride ophthalmic solution to paralyze the iris sphincter muscle. The anesthetized mouse was restrained onto a motorized stage with a scanning step size of 2 μm. The PA illumination laser pulse repetition rate was 1 kHz. We adjusted optical focal region to cover the limbus area in the cornea because neovascularization always originates from the limbal vascular plexus and then progresses toward the corneal center [30]. We imaged a 3 mm × 3 mm area to cover the whole mouse cornea. There are a total of 1500 × 1500 A-lines; each A-line comprises 200 data points; and no signal averaging was used.

It took 20 min to acquire an image with a field-of-view of 3 mm ×3 mm, which covers the whole upper corneal surface of the eye. During the imaging process, we used a lamp to keep the mouse's body warm. All of these experimental procedures were approved by Northwestern University's Institutional Animal Care and Use Committee (IACUC) and conformed to the Association for Research in Vision and Ophthalmology Statement on Animal Research.

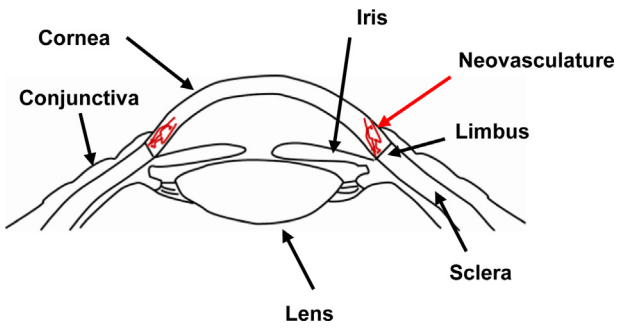

Fig. 2. Diagram of corneal structure and corneal neovascularization. For a healthy mouse cornea, there are no blood vessels; for an injured mouse cornea, there is abnormal growth of blood vessels (marked by the red arrow) from the limbus into the adjacent corneal stroma.

2.3. Immunostaining

Corneal immunostaining and flat mounting was performed as previously described [29]. Briefly, enucleated eyes were fixed in 4% paraformaldehyde (PFA) for one hour at room temperature, rinsed in PBS, and cut in half. The iris was removed from the cornea and the cornea was cut radially to facilitate flat mounting. The corneas were placed in 100% methanol at −20 °C overnight before immunostaining.

To detect blood and lymphatic vessels in flat-mount immunostaining, the corneas were permeabilized with 1% Triton X-100/PBS for 20 min, and blocked with 5% donkey serum (Sigma) for 20 minute, and then stained with anti-Lyve-1 antibodies (Abcam) overnight at 4 °C. Corneas were then washed with 0.1% Tween 20/PBS and then stained with PE-conjugated anti-CD31 (BD Biosciences, clone MEC 13.3) and AlexaFluor488 donkey anti-rabbit IgG (Invitrogen). Corneas were flat mounted and images were collected by a Zeiss Axio Observer D1 at 2.5×.

3. Results

OR-PAM images were acquired from both injured and normal wild-type C57BL6/J mouse eyes to examine the presence and prevalence of corneal neovascularization. The acquired 3D OR-PAM dataset was first smoothed by a 3 × 3 median filter within each B-scan to reduce background noise, then visualized through a maximum amplitude projection (MAP) along each A-line to form a 2D projected image. Fig. 3a shows a 3 mm by 3 mm MAP image of the whole volumetric data from an injured left eye. In Fig. 3a, the corneal vessels are not clearly visible because of the strong PA signals generated from the iris due to high melanin concentration, which can be confirmed by the cross-sectional OR-PAM B-scan image. One sample OR-PAM B-scan image selected from the highlighted position in Fig. 3a is shown in Fig. 3b, where the melanin-rich iris, represented by the solid, circular-shaped surface occupying the bottom half, is imaged below the corneal vessels (highlighted by the arrow). There is no clear visualization of the pupil in OR-PAM, as shown in Fig. 3a. One possibility could be due to inflammation accompanying corneal vascularization, which may prevent the pupil from being visible [31].

To better visualize the corneal vessels, we first identified the boundary of the iris by the strong optical absorption of the iris melanin; then, we fitted a smooth curve (as shown in Fig. 3b by the red-line) within each B-scan image to separate the iris and cornea vessels, finally we digitally removed the iris and conducted MAP operation again to highlight only optical absorption from the corneal vasculature. The result was showed in Fig. 3c, where a densely-packed vascular network is clearly visualized.

We confirmed our OR-PAM imaging results with histological corneal examination. For simplicity, we merely demonstrated the results from a small corneal region within the dash box labeled in Fig. 3c. A magnified view of selected blood vessels from the dashed-box in Fig. 3c is shown in Fig. 3d, where arrows 1–3 highlight specific vessels of interest. The measured large vessel diameter in Fig. 3d is 74 ± 6.51 μm, and the small vessel diameter is

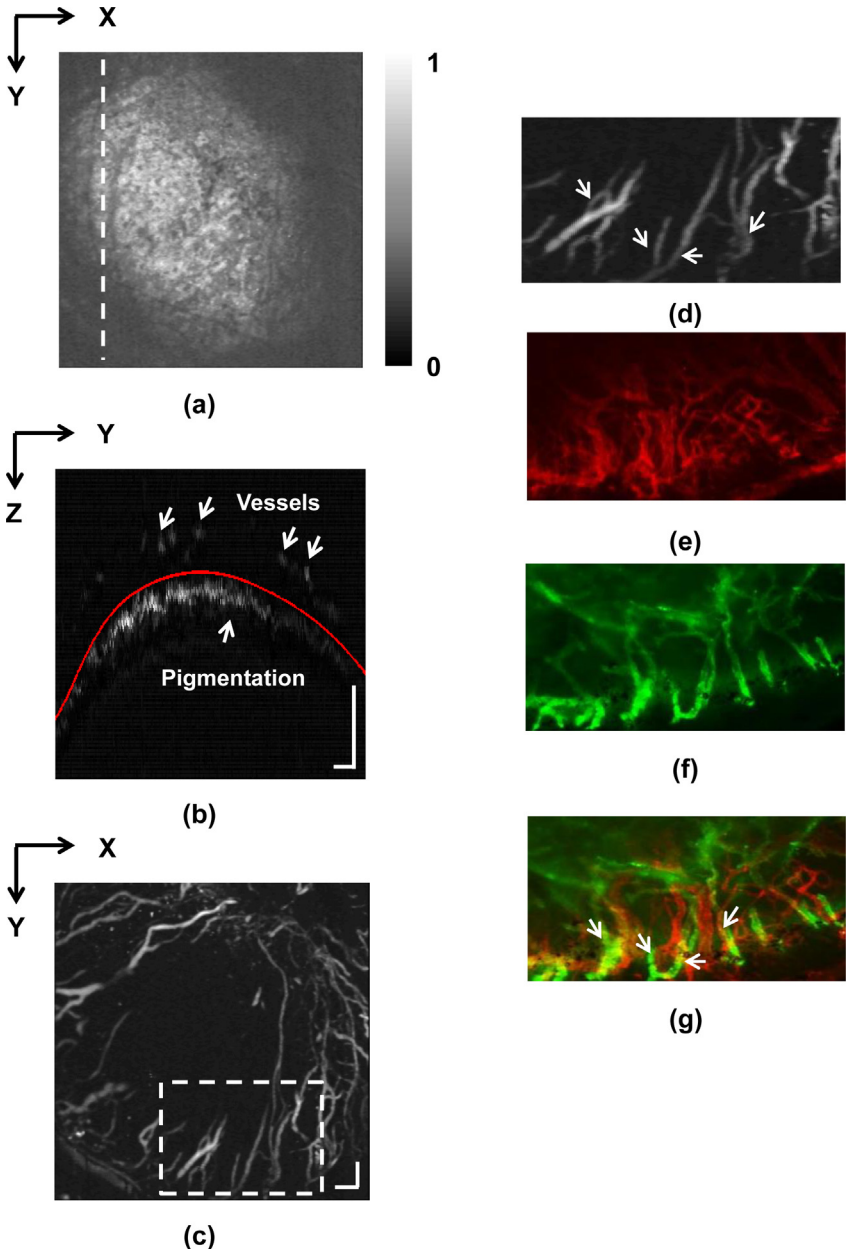

Fig. 3. Imaging results of an injured cornea. (a) Full-volume projection OR-PAM image; (b) B-scan image from the position highlighted in panel A. The overlaid red curve is the boundary of pigment-rich tissue detected by an automatic algorithm; (c) Projection after segmentation; (d) magnified view of the area enclosed by the dashed-box in panel c; (e) histological image of the area shown in (d) acquired with anti-CD31 staining, which highlights blood and lymphatic vessels; (f) histological image of the area shown in (d) stained with anti-Lyve-1 antibodies, which visualizes lymphatic vessels only; (g) fused CD31 and Lyve-1 histological images, where arrows highlight three vessels matching with magnified OR-PAM image shown in panel D. Bar: 200 μm.

28 ± 2.55 μm. Histological testing results were shown in Fig. 3e–g. In Fig. 3e, where the cornea sample was stained with PE-conjugated anti-CD31, the image was produced at a resolution of 2 μm using a commercial microscope. Since anti-CD31 highlights both blood and lymphatic vessels, a second stain was performed with anti-Lyve-1 antibodies to capture only the lymphatic vessels, which is shown in Fig. 3f. The overlaid CD31 and Lyve-1 image is shown in Fig. 3g, where the three highlighted vessels exhibit matching branching patterns as seen in Fig. 3d.

The images from a control mice cornea are shown in Fig. 4. For the healthy mice cornea, in the OR-PAM image, we can observe a dark vascular network in a bright background, which are iris vessels (highlighted by arrows) embedded in a highly pigmented background (Fig. 4a). A detailed B-scan of the normal cornea is given in Fig. 4b obtained at the position highlighted in Fig. 4a. Unlike what we can observe in Fig. 3b, there is only a continuous melanin-rich layer without any vessels present above it in Fig. 4b. The two arrows in Fig. 4b highlight shadows created by two iris vessels that can also be seen in Fig. 4a. Histological examination with anti-CD31 further confirmed the lack of corneal vascularization (Fig. 4c).

4. Discussion and conclusion

In this report we applied OR-PAM for cornea vascular imaging. OR-PAM leverages only the endogenous light absorbers in the tissue, so it is totally label free, and therefore needs no chemical dye for vascular imaging. Furthermore, with multiple wavelength imaging, the oxygen saturation could be precisely quantified through OR-PAM [21]. In the present study, where for preliminary

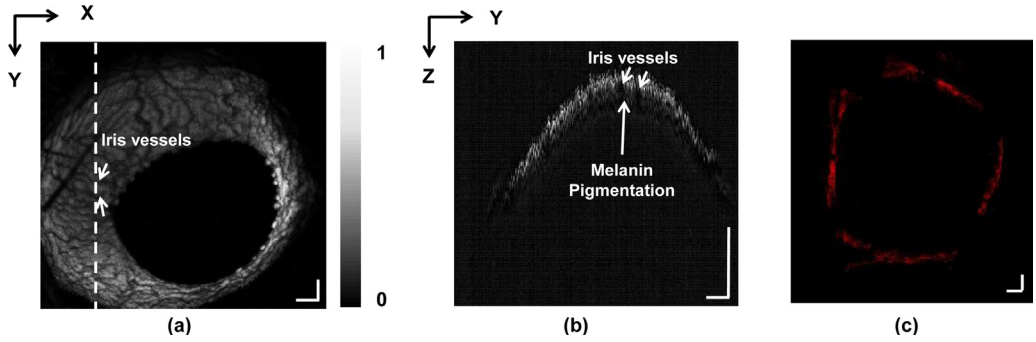

Fig. 4. Imaging results of a control eye. (a) Full-volume projection OR-PAM image, where pupil and iris vascular networks can be observed; (b) B-scan image from the location highlighted in panel A. The arrows point out shadows created by iris vessels; (c) Histological image of the whole cornea with anti-CD31 staining, which shows no blood and lymphatic vessels. Scale bar: 200 μm.

research we applied single wavelength OR-PAM for corneal vessel network imaging, we demonstrated, for the first time, OR-PAM imaging of alkali-burn-injured mouse eyes *in vivo*. Using OR-PAM, both injured and control eyes were imaged, where we clearly visualized vascular invasions into the cornea as a result of injury, further confirmed by histology. Additionally, the imaging laser pulse energy was measured to be 80 nJ, which is safe for mice eye imaging [26].

Visualization of the vascular network in the cornea *in vivo* can be important for studying the mechanism of corneal neovascularization. Comparison with previously tested imaging modalities for corneal neovascularization [4–6], OR-PAM can achieve a similar lateral resolution as confocal microscopy, while requiring no contrast agent in both anatomical and functional imaging of microvascular networks. OR-PAM can obtain a volumetric image from a two-dimensional scan combined with time-resolved ultrasonic detection. In comparison, confocal microscopy needs a three-dimensional scan to acquire the same volumetric image. More importantly, OR-PAM has the capability to quantify vascular oxygen saturation noninvasively, which will open up new possibilities in corneal angiogenesis research.

Another potential alternative for corneal neovascularization network mapping and visualization is optical coherence tomography (OCT) [32], which boasts high axial resolution, high speed, non-contact imaging, and capabilities of mapping micro-vessels in tissue through phase or speckle variance contrast. However, one of the key parameters involved in neovasculature development is the hypoxic environment [33], where variations in vessel sO_2 are still beyond the reach of existing OCT. These changes currently can only be measured precisely using photoacoustic microscopy [8,13,20], which is the motivation of this work.

There are a few limits of OR-PAM corneal neurovascular imaging. The micro-vessels span almost the entire region of the cornea, yet vascular discontinuity was observed at the corneal center as shown in Fig. 3c. This is caused by the limited imaging depth of our current OR-PAM system and the large depth variation of the corneal vessels. The imaging depth of our OR-PAM is 700 μm, while the depth variation of corneal vessels can be more than 1.4 mm owing to the curvature of the mouse cornea [28]. Such a depth range was much larger than the imaging depth of our system. During imaging, we adjusted the optical focal region to cover the area around the corneal limbus because neovascularization originates from the limbal vascular plexus and progresses toward the central cornea [30], as a result, we observed clear vasculature in the limbal areas but vascular discontinuities at or near the cornea center. To compensate for such a large depth variation due to sample curvature, we can employ a *z*-axis scan in the system as previously reported. [34]

In addition, there are several aspects that can be further refined for future studies. To improve the spatial resolution to image finer vascular network, we plan to employ ultrasonic transducers with higher center frequencies (75 MHz) to achieve finer lateral ultrasonic focusing. We can potentially integrate fluorescence confocal microscopy into OR-PAM [35,36] to image both corneal vascular and lymphatic networks at the same time after delivering an appropriate fluorescent dye into the lymphatic system. Moreover, we plan to apply multi-wavelength OR-PAM to assess the blood oxygen saturation, and further monitor the developmental progress of corneal neovascularization over time in rodent models. After achieving the proposed improvements, this novel technique will allow us to visualize corneal neovascularization in knockout animals to elucidate the underlying mechanisms of neovascularization and eventually provide guidance in treating human patients.

Conflict of interest statement

All the authors of this manuscript declare no conflict of interest of any kind. The authors alone are responsible for the content and writing of the paper.

Acknowledgements

The authors acknowledge the generous financial supports from NIH grants HL074121, HL108795 and EY019484 to TK, NIH grants 1R01EY019951 and 1RC4EY021357 to HFZ, and NSF grant CBET-1055379 to HFZ. Wenzhong Liu is a Howard Hughes Medical Institute (HHMI) international student fellow.

References

[1] Schwartz GS, Harrison AR, Holland EJ. Etiology of immune stromal (interstitial) keratitis. Cornea 1998;17(3):278–81.
[2] Gluth MB, Baratz KH, Matteson EL, Driscoll CLW. Cogan syndrome: a retrospective review of 60 patients throughout a half century. Mayo Clin Proc 2006;81(4):483–8.
[3] Chang JH, Garg NK, Lunde E, Han K-Y, Jain S, Azar DT. Corneal neovascularization: an Anti-VEGF therapy review. Surv Ophthalmol 2012;57(5):415–29.
[4] Conrad TJ, Chandler DB, Corless JM, Klintworth GK. In-vivo measurement of corneal angiogenesis with video data-acquisition and computerized image-analysis. Lab Invest 1994;70(3):426–34.
[5] Kirwan RP, Zheng Y, Tey A, Anijeet D, Sueke H, Kaye SB. Quantifying changes in corneal neovascularization using fluorescein and indocyanine green angiography. AM J Ophthalmol 2012;154(5):850–8.
[6] Yaylali V, Ohta T, Kaufman SC, Maitchouk DY, Beuerman RW. In vivo confocal imaging of corneal neovascularization. Cornea 1998;17(6):646–53.
[7] Rajadhyaksha M, Grossman M, Esterowitz D, Webb RH. In-vivo confocal scanning laser microscopy of human skin – melanin provides strong contrast. J Invest Dermatol 1995;104(6):946–52.

[8] Yao J, Maslov KI, Zhang Y, Xia Y, Wang LV. Label-free oxygen-metabolic photoacoustic microscopy in vivo. J Biomed Opt 2011;16(7):076003.
[9] Faber DJ, Mik EG, Aalders MCG, van Leeuwen TG. Light absorption of (oxy-)hemoglobin assessed by spectroscopic optical coherence tomography. Opt Lett 2003;28(16):1436–8.
[10] Zhang HF, Maslov K, Stoica G, Wang LV. Functional photoacoustic microscopy for high-resolution and noninvasive in vivo imaging. Nat Biotechnol 2006; 24(7):848–51.
[11] Song L, Maslov K, Wang LV. Section-illumination photoacoustic microscopy for dynamic 3D imaging of microcirculation in vivo. Opt Lett 2010;35(9):1482–4.
[12] Maslov K, Zhang HF, Hu S, Wang LV. Optical-resolution photoacoustic microscopy for in vivo imaging of single capillaries. Opt Lett 2008;33(9):929–31.
[13] Wang LV. Multiscale photoacoustic microscopy and computed tomography. Nat Photonics 2009;3(9):503–9.
[14] Xu MH, Wang LHV. Photoacoustic imaging in biomedicine. Rev Sci Instrum 2006;77(4).
[15] Hoelen CGA, de Mul FFM, Pongers R, Dekker A. Three-dimensional photoacoustic imaging of blood vessels in tissue. Opt Lett 1998;23(8):648–50.
[16] Yvonne-Tee GB, Rasool AHG, Halim AS, Rahman ARA. Noninvasive assessment of cutaneous vascular function in vivo using capillaroscopy, plethysmography and laser-Doppler instruments: Its strengths and weaknesses. Clin Hemorheol Microcirc 2006;34(4):457–73.
[17] Abran M, Matteau-Pelletier C, Zerouali-Boukhal K, Tardif J-C, Lesage F. Combined acoustic-photoacoustic and fluorescence imaging catheter for the detection of the atherosclerotic plaque. In: Oraevsky A, Wang LV, editors. Photons plus ultrasound: imaging and sensing 2011. Proceedings of SPIE, vol. 7899. San Francisco, CA, Jan 23–25: Conference on Photons Plus Ultrasound – Imaging and Sensing; 2011.
[18] Zemp RJ, Song L, Bitton R, Shung KK, Wang LV. Realtime photoacoustic microscopy of murine cardiovascular dynamics. Opt Express 2008;16(22): 18551–56.
[19] Zhang C, Cheng Y-J, Chen J, Wickline S, Wang LV. Label-free photoacoustic microscopy of myocardial sheet architecture. J Biomed Opt 2012;17(6): 060506.
[20] Krumholz A, Wang L, Yao J, Wang LV. Functional photoacoustic microscopy of diabetic vasculature. J Biomed Opt 2012;17(6):060502.
[21] Hu S, Gonzales E, Soetikno B, Gong E, Yan P, Maslov K, et al. Optical-resolution photoacoustic microscopy of ischemic stroke. In: Oraevsky A, Wang LV, editors. Photons Plus Ultrasound: Imaging and Sensing 2011. Proceedings of SPIE, vol. 7899. San Francisco, CA, Jan 23–25: Conference on Photons Plus Ultrasound – Imaging and Sensing; 2011.
[22] Siphanto RI, Thumma KK, Kolkman RGM, van Leeuwen TG, de Mul FFM, van Neck JW, et al. Serial noninvasive photoacoustic imaging of neovascularization in tumor angiogenesis. Opt Express 2005;13(1):89–95.
[23] Rao B, Li L, Maslov K, Wang L. Hybrid-scanning optical-resolution photoacoustic microscopy for in vivo vasculature imaging. Opt Lett 2010;35(10): 1521–3.
[24] Ormerod LD, Abelson MB, Kenyon KR. Standard models of corneal injury using alkali-immersed filter disks. Invest Optom Vis Sci 1989;30(10):2148–53.
[25] Xie Z, Jiao S, Zhang HF, Puliafito CA. Laser-scanning optical-resolution photoacoustic microscopy. Opt Lett 2009;34(12):1771–3.
[26] Hu S, Rao B, Maslov K, Wang LV. Label-free photoacoustic ophthalmic angiography. Opt Lett 2010;35(1):1–3.
[27] Xu M, Wang LV. Photoacoustic imaging in biomedicine. Rev Sci Instrum 2006;77(4):041101.
[28] Schmucker C, Schaeffel F. A paraxial schematic eye model for the growing C57BL/6 mouse. Vision Res 2004;44(16):1857–67.
[29] Seo S, Singh HP, Lacal PM, Sasman A, Fatima A, Liu T, et al. Forkhead box transcription factor FoxC1 preserves corneal transparency by regulating vascular growth. Proc Natl Acad Sci U S A 2012;109(6):2015–20.
[30] Kenyon BM, Browne F, D'Amato RJ. Effects of thalidomide and related metabolites in a mouse corneal model of neovascularization. Exp Eye Res 1997;64(6):971–8.
[31] Zhang ZH, Ma JX, Gao GQ, Li CY, Luo LH, Zhang M, et al. Plasminogen kringle 5 inhibits alkali-burn-induced corneal neovascularization, *Invest*. Optom Vis Sci 2005;46(11):4062–71.
[32] Walther J, Gaertner M, Cimalla P, Burkhardt A, Kirsten L, Meissner S, et al. Optical coherence tomography in biomedical research. Anal Bioanal Chem 2011;400(9):2721–43.
[33] Risau W. Mechanisms of angiogenesis. Nature 1997;386(6626):671–4.
[34] Zhang HF, Maslov K, Wang LV. Automatic algorithm for skin profile detection in photoacoustic microscopy. J Biomed Opt 2009;14(2):024050.
[35] Wang Y, Maslov K, Kim C, Hu S, Wang LV. Integrated photoacoustic and fluorescence confocal microscopy. IEEE Trans Biomed Eng 2010;57(10): 2576–8.
[36] Zhang X, Jiang M, Fawzi AA, Li X, Shung KK, Puliafito CA, et al. Simultaneous dual molecular contrasts provided by the absorbed photons in photoacoustic microscopy. Opt Lett 2010;35(23):4018–20.

Wenzhong Liu completed his B.S. in Biomedical Engineering from Tian Jin University, Tian Jin, China in 2008, and earned his M.S. in Biomedical Engineering from Shanghai Jiao Tong University, Shanghai, China in 2011. He is currently a Ph.D. candidate and a HHMI International Student Research Fellow in the Department of Biomedical Engineering at Northwestern University. He is interested in functional imaging of the eye.

Kathryn M. Schultz completed a B.S. degree in Biochemistry at the University of Illinois at Urbana-Champaign in 2004. She then began working at the Feinberg School of Medicine at Northwestern University in the Feinberg Cardiovascular Research Institute. Initially studying cell cycle regulation and cardiac regeneration, her focus has now moved to corneal development and angiogenesis.

Kevin Zhang completed his B.S. in Biomedical Engineering at Northwestern University in 2013. He remained at Northwestern University as a graduate research assistant and is currently a M.S. candidate in the Department of Biomedical Engineering. His research interests include optical imaging as it applies to biomedical fields, particularly the utilization of photoacoustics toward visualizing optical absorption contrast. His future plans include pursuing an MD/PhD degree.

Amy Sasman completed her B.S. in Pharmacology and Toxicology at the University of Wisconsin-Madison in 2006. She was then accepted to the Medical College of Wisconsin, where she earned her M.S. in Pharmacology and Toxicology in 2010. After completing her M.S. degree, Amy worked at Northwestern University, where her research focused on the role of the Forkhead box transcription factors, Foxc1 and Foxc2, in the development of the eye and cardiovascular network. She is currently employed at the Medical College of Wisconsin as a Research Associate in the Department of Pediatrics.

Fengli Gao completed his B.S. in Electronic Engineering at Jilin university, Changchun, China in 2001. He subsequently completed his M.S. and Ph.D. degrees in the College of Electronic Science and Engineering at Jilin University in 2004 and 2008, respectively. In 2010 and 2011, he joined the Functional Optical Imaging Laboratory (FOIL) at University of Wisconsin-Milwaukee and Northwestern University, where he was a postdoctoral associate and learnt about photoacoustic imaging. He currently is an Associate Professor in the College of Electronic Science and Engineering at Jilin University. His research interests include weak signal detection and semiconductor laser diodes reliability and their applications.

Tsutomu Kume received a Ph.D. degree in Molecular and Cellular Biology from the University of Tokyo in 1996. He completed his postdoctoral training in developmental biology in the lab of Brigid Hogan at the Howard Hughes Medical Institute at Vanderbilt University Medical Center. Currently he is Associate Professor at the Feinberg School of Medicine at Northwestern University. He is a Fellow of the American Heart Association. His research interests include cardiovascular development, cardiovascular stem/progenitor cells, and developmental/pathological angiogenesis.

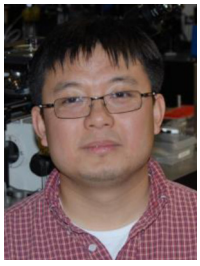

Hao F. Zhang received his Ph.D. in Biomedical Engineering from Texas A&M University, College Station, TX in 2006. From 2006 to 2007, he was a post-doctoral fellow at Washington University in St. Louis, St. Louis, MO. He is currently an Associate Professor in the Department of Biomedical Engineering and Department of Ophthalmology at Northwestern University, Evanston, IL. His research interests include optical microscopy, nonlinear optics, laser-tissue interaction, retinal imaging, and image processing.